The Dynamics of an Optimally Controlled Tumor Model: A Case Study

L. G. DE PILLIS
Harvey Mudd College, Claremont, CA 91711, U.S.A.
depillis@math.hmc.edu

A. RADUNSKAYA
Pomona College, Claremont, CA 91711, U.S.A.
aradunskaya@pomona.edu

Abstract—We present a phase-space analysis of a mathematical model of tumor growth with an immune response and chemotherapy. We prove that all orbits are bounded and must converge to one of several possible equilibrium points. Therefore, the long-term behavior of an orbit is classified according to the basin of attraction in which it starts. The addition of a drug term to the system can move the solution trajectory into a desirable basin of attraction. We show that the solutions of the model with a time-varying drug term approach the solutions of the system without the drug once treatment has stopped. We present numerical experiments in which optimal control therapy is able to drive the system into a desirable basin of attraction, whereas traditional pulsed chemotherapy is not. © 2003 Elsevier Science Ltd. All rights reserved.

Keywords—Cancer, Tumor, Population models, Competition models, Mathematical modelling, Immune system, Optimal control, Ordinary differential equations.

1. INTRODUCTION

A tumor's response to treatment depends on many factors, including the severity of the disease, the application of the treatment, and the strength of patient's own immune response. Mathematical modelling of this process is viewed as a potentially powerful tool in the development of improved treatment regimens. The mathematical modelling of tumor growth and treatment has been approached by a number of researchers using a variety of models over the past decades. In this current work, we expand upon an earlier model that we developed [1], in which tumor growth, an immune response, and chemotherapy treatment are represented by a system of four differential equations.

Our representation extends other lower-dimensional models, such as that described in [2], in which different cell populations are represented as interacting species. Other mathematical models that include an immune interaction with a tumor are described in [3–11]. The model includes a variable representing the concentration of a cytotoxic agent at the tumor site, similar to the approach used in [12–21]. We have shown that optimal control could be used to describe treatment protocols which have the potential to be more efficient than standard periodic protocols

now in use. Optimizing chemotherapy treatments using mathematical models has also been explored in the works of [22–36] and more recently in [37–42].

The goal of our earlier work was to refine previous models and to apply the theory of optimal control to this more refined model. Our results suggested that, in order to keep oscillations in the cell populations to a minimum, a further exploration of the types of objective functions was warranted. Here, we present new results of optimal control experiments implementing a more flexible set of objective functions. Additionally, we find that if we can move the system into the basin of attraction of a healthy, stable equilibrium state, treatment can be discontinued, while the system continues to move toward the disease-free state. This motivates us to carry out a detailed phase-space analysis of our model in order to have a more complete understanding of the implications of the existence of basins of attraction in the treatment process.

1.1. Phase Space Analysis

Phase space analysis has been used successfully in the study of two-dimensional population models. For example, in [2], a detailed description of the orbit structure of a two-dimensional population model of tumor and immune cells is given which provides a possible explanation of observed clinical phenomena such as creeping through, oscillations in tumor size, remission, and tumor recurrence. In addition, the dependence of the structure of phase space on system parameters was studied which produced a bifurcation diagram in parameter space. Other two-dimensional models which include the effect of chemotherapy [6,17,43] have also been analyzed from a phase-space point of view. See, also [44] where a four-dimensional model of immunotherapy is analyzed.

The typical strategy in a phase-space analysis of a smooth system of differential equations begins with the identification of limit sets and their stability. In two dimensions, the limit set of any orbit falls into one of three categories: it is either an equilibrium, or a cycle, or the orbit is unbounded. The question of the existence of cycles can be answered using Lyapunov techniques, or by theorems such as the Poincaré-Bendixson theorem and Dulac's criterion, which are applicable only in two dimensions. For example, in [2], Dulac's criterion is used to eliminate the possibility of periodic orbits, although oscillating tumor populations might still be observed in the neighborhood of a spiral sink. Unfortunately, the structure of higher-dimensional phase-space can be much more complicated. In three dimensions, for example, it is possible for the limit set of an orbit to be a two- or three-dimensional bounded invariant set containing no periodic orbits, i.e., a strange attractor. In [44], a four-dimensional model is discussed which can undergo Hopf bifurcations leading to periodic orbits, a possible route to the development of chaotic attractors. Furthermore, fewer theorems are available which can ensure or exclude the existence of periodic orbits, although Lyapunov functions can sometimes be found which ensure the global stability of an attractor, as is done in [44]. For this reason, it is of interest to provide a complete analysis of a three-dimensional system as an example of a geometric technique which might be generalized to other systems. In particular, a description of null-surfaces of the vector field can be useful in the characterization of the long term behavior of all orbits. In [45–50], purely competitive three-dimensional population models are classified using the null-surfaces, which in these models are given by planes in the positive octant. For example, in [49] it is shown that all orbits approach an invariant surface, so that the problem is essentially reduced to a two-dimensional one. While the model described here is not purely competitive, so that the null-surfaces are not simple planes, the geometric approach proves to be fruitful.

This paper is structured as follows. First, for the convenience of the reader, we briefly review the development of the model from [1]. We discuss the existence of equilibria and their stability in a range of model parameters. We then perform a case study for a specific parameter set, illustrating the geometric techniques for analyzing the phase-space of the system. In order to apply these results to a model which includes chemotherapy, we verify that the solutions to the

system with a time-varying drug concentration are asymptotic to solutions of the autonomous, drug-free system. Then, we present numerical solutions to an optimal control problem, which illustrate the benefit of moving a system into a healthy basin of attraction early on in treatment.

2. THE MODEL

Our model has the following components.

- *Immune response.* The model includes immune cells whose growth may be stimulated by the presence of the tumor and that can destroy tumor cells through a kinetic process. We point out that the presence of a detectable tumor in a system does not necessarily imply that the tumor has completely escaped active immunosurveillance. It is entirely possible that although a tumor is immunogenic, the immune system response is not sufficient on its own to completely combat the rapid growth of the tumor cell population and the eventual development into a tumor. In fact, there is even some speculation that all tumors are immunogenic; see, for example, [51].
- *Competition terms.* Normal cells and tumor cells compete for available resources, while immune cells and tumor cells compete in a predator-prey fashion.
- *Optimal control theory for chemotherapy.* A set of optimal drug therapies is calculated that minimize both the final tumor population, as well as the average tumor population over time, while keeping the normal cells above a required level; these solutions are then used to design a practical treatment protocol.

We focus on tissue near the tumor site, and we assume a homogeneous tumor. We choose to model the reaction of the immune cells with the tumor cells in the same manner as that described in [2]. For the growth law terms, we considered several possible models, including exponential growth, Gompertz growth, and logistic growth. Over the past several decades, various authors have argued for the superiority of each of these growth laws in different contexts, and for different types of cancers, see, e.g., [52,53]. However, since the model we discuss here is intended to be qualitative and does not focus on a particular tumor type, it is not immediately apparent how to measure which growth law is preferable in this context. It turns out, however, that the growth law terms we compared allow for similar growth behavior up to a certain point in tumor size. For our particular set of experiments, the choice of growth law does not significantly affect the qualitative behavior of the model. For the present, therefore, we use a logistic growth term. We present analytic and numerical analysis of this new model, as well as open questions and future directions for refining the model.

Preliminary numerical results have already suggested that standard treatment protocols may not be optimal and that better outcomes may be achieved by administering medication in ways that have not been previously employed clinically. As this new model is developed and refined, these theories can be more thoroughly tested. Although there is still much to be done to test the new theories, every new result has the potential to be an advance toward improving the quality of treatment for cancer sufferers.

2.1. The Model—Equations

We let $I(t)$ denote the number of immune cells at time t, $T(t)$ the number of tumor cells at time t, and $N(t)$ the number of normal, or host, cells at time t.

The source of the immune cells is considered to be outside of the system so it is reasonable to assume a constant influx rate s. Furthermore, in the absence of any tumor, the cells will die off at a *per capita* rate d_1, resulting in a long-term population size of s/d_1 cells. Thus, immune cell proliferation will never suffer from immune upon immune crowding. The presence of tumor cells stimulates the immune response, represented by the positive nonlinear growth term for the immune cells

$$\frac{\rho I(t)T(t)}{\alpha + T(t)}, \tag{2.1}$$

where ρ and α are positive constants. This type of response term is of the same form as the terms used in the respective models of Kuznetsov *et al.* [2] and Kirschner and Panetta [7]. It is also similar to the one used by Owen and Sherratt [43] once their system is reduced to the pseudo-steady state. In particular, as a function of T, it is positive, increasing, and concave.

Furthermore, the reaction of immune cells and tumor cells can result in either the death of tumor cells or the inactivation of the immune cells, represented by the two competition terms

$$\frac{dI}{dt} = -c_1 I(t)T(t) \qquad \text{and} \qquad \frac{dT}{dt} = -c_2 I(t)T(t). \tag{2.2}$$

As discussed at the beginning of this section, the tumor cells as well as the normal cells are modelled by a logistic growth law, with parameters r_i and b_i representing the *per capita* growth rates and reciprocal carrying capacities of the two types of cells: $i = 1$ identifies the parameters associated with the tumor, and $i = 2$ identifies those associated with the normal tissue. In addition, there are two terms representing the competition between tumor and host cells.

Putting all the terms together gives the following system of ordinary differential equations:

$$\dot{N} = r_2 N(1 - b_2 N) - c_4 TN,$$
$$\dot{T} = r_1 T(1 - b_1 T) - c_2 IT - c_3 TN, \tag{2.3}$$
$$\dot{I} = s + \frac{\rho IT}{\alpha + T} - c_1 IT - d_1 I.$$

The behavior of this system without drug interactions will be analyzed in Sections 3 and 4.

We now add the effect of the drug on the system. We denote by $u(t)$ the amount of drug at the tumor site at time t. We assume that the drug kills all types of cells, but that the kill rate differs for each type of cell, with the response curve in all cases given by an exponential

$$F(u) = a\left(1 - e^{-ku}\right), \tag{2.4}$$

where $F(u)$ is the fractional cell kill for a given amount of drug u, at the tumor site. Since the details of the pharmacokinetics are unknown, we let $k = 1$ in these preliminary studies. We denote by a_1, a_2, and a_3 the three different response coefficients. We add these terms to the system of differential equations above as well as an equation for $u(t)$, the amount of drug at the tumor site. This is determined by the dose given $v(t)$, and a *per capita* decay rate of the drug once it is injected. This decay rate incorporates all pathways of elimination of the drug. The system with drug interaction is then given by

$$\dot{N} = r_2 N(1 - b_2 N) - c_4 TN - a_3(1 - e^{-u})N,$$
$$\dot{T} = r_1 T(1 - b_1 T) - c_2 IT - c_3 TN - a_2(1 - e^{-u})T,$$
$$\dot{I} = s + \frac{\rho IT}{\alpha + T} - c_1 IT - d_1 I - a_1(1 - e^{-u})I, \tag{2.5}$$
$$\dot{u} = v(t) - d_2 u.$$

3. DRUG-FREE EQUILIBRIA

To better understand the dynamics of the system, we first analyze the system without any drug input ($u(t) = 0$ for all t). In order to consider the patient "cured", the system must be either in the basin of a stable tumor-free equilibrium or in the basin of a stable equilibrium at which only a harmlessly small amount of tumor is present.

The three sets of null-surfaces of the drug-free system given by (2.3) are described by the following:

- $\tilde{N}_N$

$$\dot{N} = 0 \Rightarrow \begin{cases} N = 0, & (I - T \text{ coordinate plane}), \text{ or} \\ N = \dfrac{1}{b_2} - \left(\dfrac{c_4}{r_2}\right)T, & (\text{Plane } N_N). \end{cases} \tag{3.1}$$
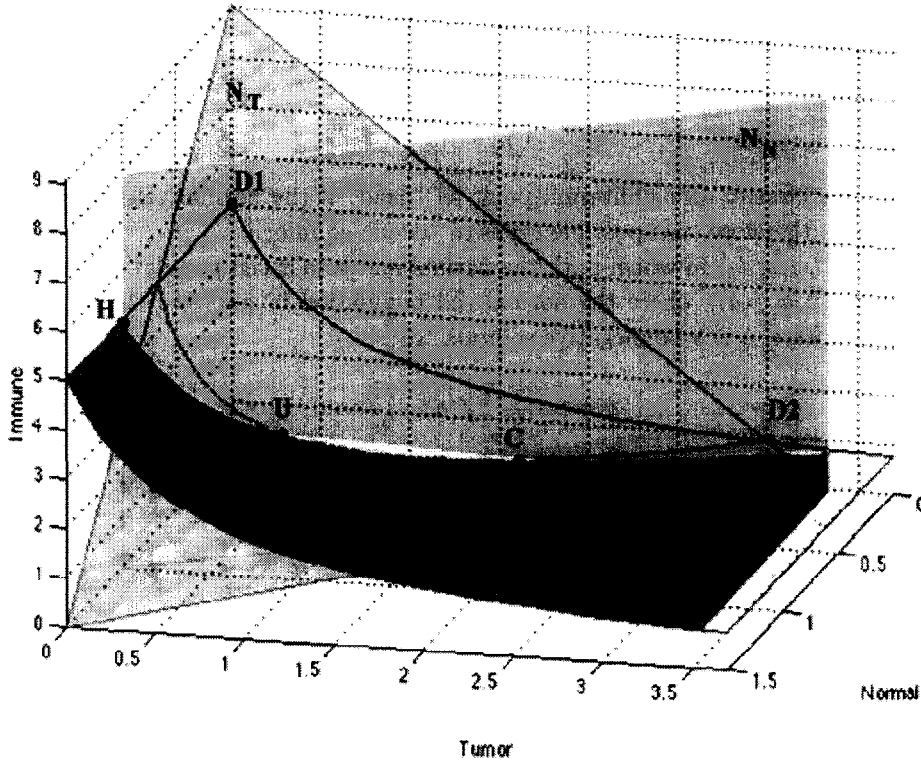
Figure 1. The three null-surfaces in the positive octant with the equilibria marked: H is the "healthy" tumor-free equilibrium, U is the unstable interior equilibrium, C is the "unhealthy" interior stable equilibrium, and D1 and D2 are the two unstable "dead" equilibria, where there are no normal cells.

$\tilde{N}_N$ is a union of two planes, the I-T coordinate plane and N_N, a plane parallel to the I-axis. Letting $g(T)$ be a function describing N_N in terms of the tumor population, we define

$$g(T) \equiv \frac{1}{b_2} - \left(\frac{c_4}{r_2}\right) T. \tag{3.2}$$

- $\tilde{N}_T$

$$\dot{T} = 0 \Rightarrow \begin{cases} T = 0, & (I\text{-}N \text{ coordinate plane), or} \\ T = \frac{1}{b_1} - \left(\frac{c_2}{r_1 b_1}\right) I - \left(\frac{c_3}{r_1 b_1}\right) N, & (\text{Plane } N_T). \end{cases} \tag{3.3}$$

$\bar{N}_T$ is also a union of two planes, the I-N coordinate plane, and the plane we will call N_T.
- $\tilde{N}_I$

$$\dot{I} = 0 \Rightarrow I = \frac{s(\alpha + T)}{(c_1 T + d_1)(\alpha + T) - \rho T}, \tag{3.4}$$

as long as $\rho T \neq (c_1 T + d_1)(\alpha + T)$.

N_I is a curved cylindrical surface parallel to the N-axis. Letting $f(T)$ be a function of the tumor population T, we let $f(T)$ describe N_I by defining

$$f(T) \equiv \frac{s(\alpha + T)}{c_1 T(\alpha + T) + d_1(\alpha + T) - \rho T}. \tag{3.5}$$

The null-surfaces for the particular set of parameter values used in our experiments are pictured in Figure 1. See Section 4 for a list of parameter values. The types of equilibrium points that could occur at the intersections of these surfaces can be classified as follows.

- *Tumor-free.* In this category, the tumor cell population is zero but the normal cells survive The equilibrium point has the form

$$\left(\frac{1}{b_2}, 0, \frac{s}{d_1} \right).$$

(3.6)

- *Dead.* We classify an equilibrium point as "dead" if the normal cell population is zero. There are, therefore, two possible types of "dead" equilibria.

  Type 1. $(0, 0, s/d_1)$ in which both the normal and tumor cell populations are zero, and

  Type 2. $(0, a, f(a))$ where the normal cell population is zero and the tumor cells have survived. Here, a is a nonnegative solution to

$$a + \left(\frac{c_2}{r_1 b_1} \right) f(a) - \frac{1}{b_1} = 0.$$

(3.7)

- *Coexisting.* Here, both normal and tumor cells coexist with nonzero populations. The equilibrium point is given by

$$(g(b), b, f(b)),$$

(3.8)

where b is a nonnegative solution of

$$b + \left(\frac{c_2}{r_1 b_1} \right) f(b) + \left(\frac{c_3}{r_1 b_1} \right) g(b) - \frac{1}{b_1} = 0.$$

(3.9)

Depending on the values of these parameters, there could be zero, one, two, or three of these equilibria. The two equilibrium states that the system should ideally approach, in the context of developing treatment therapy, are the tumor-free equilibrium and any coexisting equilibrium for which b is small and $g(b)$ is close to 1, since in these states, the normal cell population is close to its healthy state.

3.1. Tumor-Free Equilibrium

In principle, we would like the tumor-free equilibrium to be stable so that the possibility exists of moving the state of the system toward the tumor-free point. In this section, we discuss for which parameter ranges the tumor-free equilibrium is locally stable. Linearization around this equilibrium gives the system

$$\begin{bmatrix} \dot{N} \\ \dot{T} \\ \dot{I} \end{bmatrix} = \begin{bmatrix} r_2 - 2r_2 b_2 & -c_4 & 0 \\ 0 & r_1 - \dfrac{c_2 s}{d_1} - c_3 & 0 \\ 0 & \dfrac{\rho s}{d_1 \alpha} - \dfrac{c_1 s}{d_1} & -d_1 \end{bmatrix} [N, T, I],$$

(3.10)

with eigenvalues

$$\lambda_1 = r_2 - 2r_2 b_2, \qquad \lambda_2 = r_1 - \frac{c_2 s}{d_1} - c_3, \qquad \lambda_3 = -d_1 < 0.$$

(3.11)

Thus, the tumor-free equilibrium is stable as long as λ_1 and λ_2 are negative. If $1 - 2b_2 < 0$, then $\lambda_1 < 0$. In our simulations, the normal cell population is normalized so that $b_2 = 1$, hence, λ_1 is negative.

$$\lambda_2 < 0 \Rightarrow r_1 < \frac{c_2 s}{d_1} + c_3.$$

(3.12)

This relates the *per capita* growth rate of the tumor cells r_1, to the "resistance coefficient", $c_2 s/d_1$, which measures how efficiently the immune system competes with the tumor cells. If this tumor-free equilibrium is unstable, then according to this model, no amount of chemotherapy will be able to completely eradicate the tumor. This is, in fact, the case in the model of [43] for all parameter values.

3.2. Dead Equilibria

The same type of analysis as above shows that the Type 1 dead equilibrium at $(0, 0, s/d_1)$ is always unstable. The Type 2 dead equilibrium at $(0, a, f(a))$ can be either stable or unstable, depending on the parameters of the system. For any particular set of parameter values, one could apply the Routh test (see, for example, [54, p. 415]) to the characteristic polynomial of the Jacobian. For the parameter set used in our optimal control experiments, the Type 2 dead equilibrium is located approximately at $(0, 0.89924, 0.302268)$ and is unstable.

3.3. Coexisting Equilibria

Also of interest are the existence and stability of equilibria where a small tumor mass might coexist with a large number of normal cells. These equilibria occur at the intersection of the components of the three null-surfaces that do not correspond to coordinate planes. Figure 1 shows the lines of intersection of these surfaces. The three curves of intersection meet at two points, the coexisting equilibria, which are marked on the graph.

As stated depending on the parameter values, there can be zero, one, two, or three of these equilibria. The null-surfaces divide the positive octant into at most 12 regions. The goal of chemotherapy is to get the system into a region of stability of one of the "harmless" equilibria: either the tumor-free equilibrium at $(1, 0, s/d_1)$ or an equilibrium at which only a small amount of tumor is present. The basins of attraction for a special case study will be discussed in more detail in Section 4.4.

Figure 2 shows the existence and stability of these equilibria as a function of the immune response rate ρ, and the immune source rate s. All other parameter values are set to be equal to those used in our later experiments. For our parameter values with $\rho = 0.01$ and $s = 0.33$, there
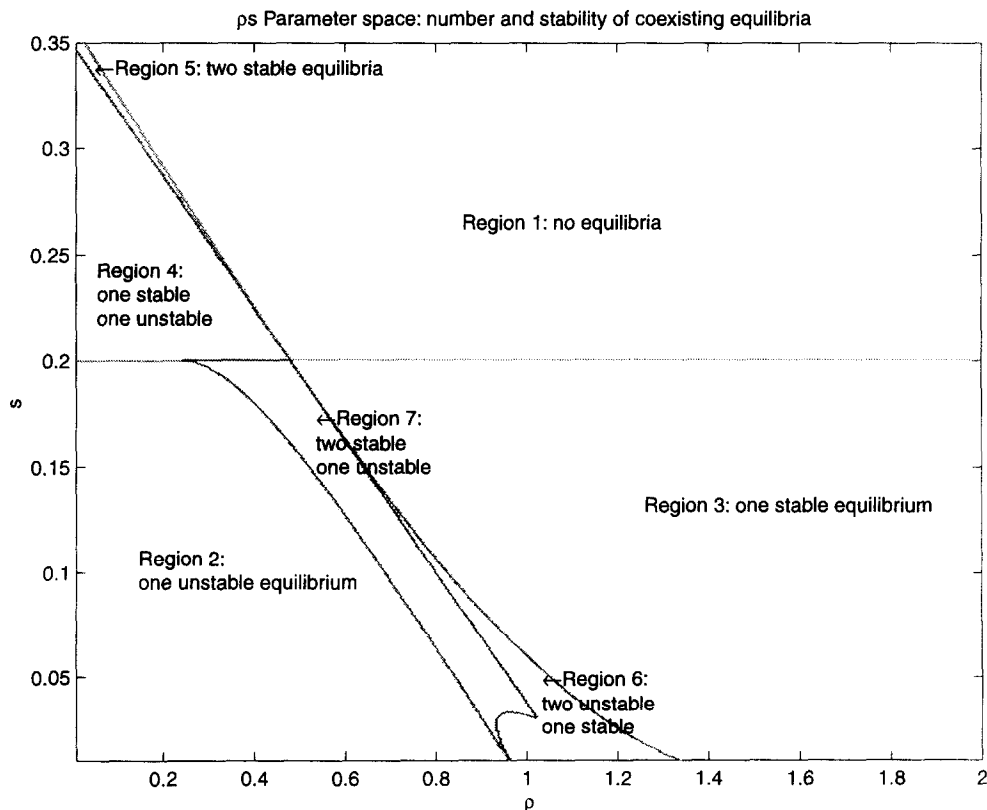

Figure 2. Coexisting equilibria as a function of source rate s and immune response ρ.

are two coexisting equilibria, one is stable and one is unstable. That is, our experimental parameter values place us in Region 4.

4. CASE STUDY IN NORMAL PARAMETER RANGE

For the particular parameter set we introduce in this section, we have two unstable dead equilibria, one stable coexisting equilibrium at $I = 0.44$, $T = 0.56$, $N = 0.44$, and a stable tumor free equilibrium at $N = 1.0$, $T = 0.0$, $I = 1.65$.

The exact parameters we use are

$$a_1 = 0.2, \qquad a_2 = 0.3, \qquad a_3 = 0.1, \qquad b_1 = 1.0, \qquad b_2 = 1.0,$$
$$\alpha = 0.3, \qquad c_1 = 1.0, \qquad c_2 = 0.5, \qquad c_3 = 1.0, \qquad c_4 = 1.0, \tag{4.1}$$
$$d_1 = 0.2, \qquad d_2 = 1.0, \qquad r_1 = 1.5, \qquad r_2 = 1.0, \qquad s = 0.33, \qquad \rho = 0.01.$$

4.1. Description of Parameters

In this section, we summarize the parameters of our mathematical model in lexicographic order. This parameter set may vary from case to case. However, the ideas of the analysis we present are sufficiently general that they still apply. So the question we ultimately ask is this: given a particular set of parameter values (as outlined below), what does our analysis reveal about the behavior of the system?

Recall that the units of cells were rescaled, so that one unit represents the carrying capacity of the normal cells in the region of the tumor. This depends on the type of tumor, of course, but it is reasonable to allow this to be on the order of 10^{11} cells [55]. If one assumes that there are between 10^8 and 10^9 cells per cubic centimeter of tissue, then the normal cell population at carrying capacity encompasses a volume with a diameter somewhere between 5.8 and 12.4 centimeters. The parameter ranges implemented are as follows.

- *Fraction cell kill.* $0 \leq a_i \leq 0.5$, with $a_3 \leq a_1 \leq a_2$. In our experiments, these numbers were considered variable, in the sense that different drugs provide for different cell kill rates. On the other hand, we wanted to avoid unreasonably efficient drugs, hence the upper bound of 0.5 on all the values.
- *Carrying capacities.* $b_1^{-1} \leq b_2^{-1} = 1$.
- *Competition terms.* c_1, c_2, c_3, c_4 are taken to be positive in these experiments. Some authors argue that c_3 might be negative, and there is some clinical evidence for this [8,17]. A negative competition coefficient in this case would imply that instead of the normal cells destructively competing with the tumor cells for resources and space, the presence of the normal cells would in fact stimulate further growth of the tumor cell population. In these preliminary experiments, however, we assume destructive competition.
- *Death rates.* d_1 and d_2. Here, d_1 is the *per capita* death rate of the immune cells, with $d_1 = 0.2$, and d_2 is *per capita* death rate of the drug, with $d_2 = 1$.
- *Per unit growth rates.* r_1 and r_2, with time normalized so that $r_2 = 1$. Depending on the type of cancer and the stage of growth, r_1 may be bigger or smaller than r_2. See, for example, [56–58]. Here, we assume that the tumor cell population grows more rapidly than the normal cell population, and let $r_1 > r_2$.
- *Immune source rate.* s, a steady source rate for immune cells in the absence of a tumor. In our experiments, $0 \leq s \leq 0.5$, see [2].
- *Immune threshold rate.* α, which is inversely related to the steepness of the immune response curve. When the number of tumor cells T is equal to α, the immune response rate is at half of its maximum value. We used $\alpha = 0.3$. See, for example, the parameter estimation work in [2].
- *Immune response rate.* ρ, which we assume to have a baseline value of 1. With the other parameter choices, an interesting range of ρ is the interval $(0, 2.5)$. In [1], ρ was

varied throughout this range to determine bifurcations in the behavior of the system of equations (2.5). In the case study below, we set $\rho = 0.01$ to simulate a patient with a compromised immune system.

In the numerical experiments described in Section 7, the initial immune level is quite small, depicting again a compromised immune system. The healthy steady-state immune level is given in this model by $I = s/d_1 = 1.65$ for these parameter values. We will start at two different immune levels: $I(0) = 0.15$ and $I(0) = 0.10$, levels under 10% of the healthy level. For these experiments, we start with a relatively large tumor burden: $T(0) = 0.25$. This corresponds to a tumor with approximately 0.25×10^{11} cells, or a sphere of radius between 1.8 and 3.9 centimeters. The clinical detection threshold for a tumor is generally 10^7 cells [13], so the initial tumor volume of 0.25 normalized units is above clinical detection levels. Note that the presence of a preoperative clinically detectable tumor does not necessarily imply that the tumor has completely escaped immunosurveillance, simply that the immune system response was not sufficient to curtail the rapid growth of the tumor cell population.

Results from numerical experiments follow in Section 7.

4.2. Nondimensionalization

For the sake of simplifying the analysis, we first nondimensionalize our equations. We set the following equalities:

$$\overset{*}{N} = \hat{N}N, \qquad \overset{*}{T} = \hat{T}T, \qquad \overset{*}{I} = \hat{I}I, \qquad \overset{*}{t} = \hat{t}t, \tag{4.2}$$

where the starred quantities are nondimensional. We let $\hat{I} = r_2/s$, $\hat{T} = 1/\alpha$, $\hat{N} = b_2$, and $\hat{t} = r_2$ and substitute back into our drug-free differential equations (2.3). Then, we find that it is convenient to set

$$\overset{*}{\rho} = \frac{\rho}{r_2}, \qquad \overset{*}{c_1} = \frac{\alpha c_1}{r_2}, \qquad \overset{*}{c_2} = \frac{c_2 s}{r_2^2}, \qquad \overset{*}{c_3} = \frac{c_3}{b_2 r_2},$$

$$\overset{*}{c_4} = \frac{\alpha c_4}{r_2}, \qquad \overset{*}{d} = \frac{d_1}{r_2}, \qquad \overset{*}{r} = \frac{r_1}{r_2}, \qquad \overset{*}{b} = \alpha b_1. \tag{4.3}$$

Dropping the star-notation, our nondimensionalized system becomes

$$\begin{aligned}
\dot{N} &= N(1 - N) - c_4 TN, \\
\dot{T} &= rT(1 - bT) - c_2 IT - c_3 TN, \\
\dot{I} &= 1 + \frac{\rho IT}{1 + T} - c_1 IT - dI.
\end{aligned} \tag{4.4}$$

For clearer notation, let the size of the cell populations be denoted by

$$\begin{aligned}
x(t) = N(t) &= \text{ normal cell population at time } t, \\
y(t) = T(t) &= \text{ tumor cell population at time } t, \\
z(t) = I(t) &= \text{ immune cell population at time } t.
\end{aligned} \tag{4.5}$$

The nondimensionalized form of system (2.3) is then given by

$$\begin{aligned}
\dot{x} &= x(1 - x) - c_4 xy, \\
\dot{y} &= ry(1 - by) - c_2 yz - c_3 xy, \\
\dot{z} &= 1 + \frac{\rho yz}{1 + y} - c_1 yz - dz.
\end{aligned} \tag{4.6}$$

4.3. The Structure of Limit Sets

In this section, we prove the following.

PROPOSITION 1. *All orbits of system (4.6) with the parameter set (4.1) with initial values in the positive octant have exactly one of the equilibria as their limit set. In particular, all orbits are bounded and the system admits no nontrivial periodic orbits.*
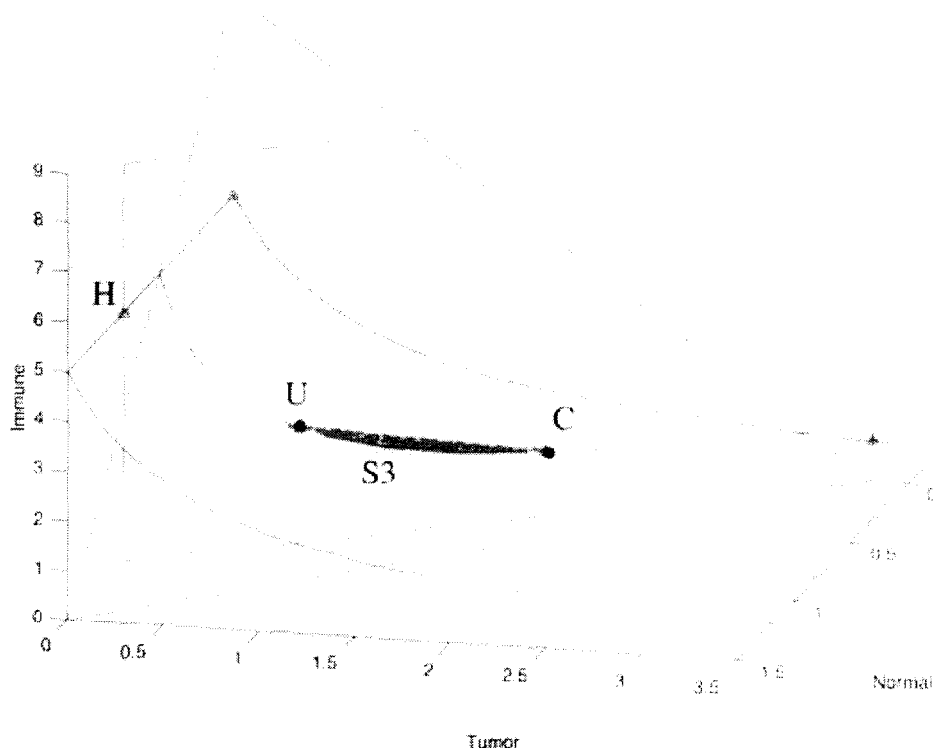
Figure 3. The small inner trapping region S_3.

General description of the limit sets

As discussed in Section 3, the system has two stable equilibria, H and C, as well as three unstable equilibria, D_1, D_2, and U. When the system is linearized about D_2, only one eigenvalue has positive real part, and the other two have negative real parts. By the stable manifold theorem (see, for example, [59]), D_2 has a two-dimensional stable manifold. The same holds for the interior unstable equilibrium U. The stable manifold of D_2 is the xz-plane, while the stable manifold of U intersects the interior of the positive octant. On the other hand, $D_1 = [0, 0, 1/d]$ has a one-dimensional stable manifold, the z-axis, since linearization about this equilibrium results in a Jacobian with only one eigenvalue with negative real part. With the exception of these three unstable equilibria and their stable manifolds, all other points in the positive octant are in the basin of attraction of one of the two stable equilibria, H or C.

PROOF OF PROPOSITION 1. We prove the proposition by showing that all orbits converge to one of the five equilibria. Since the derivatives in system (4.6) are continuous, they can only change sign along an orbit if the orbit crosses a null-surface. So, we divide the positive octant into regions in which $\dot{x}$, $\dot{y}$, and $\dot{z}$ are of constant sign: the boundaries of these regions are the null-surfaces described in Section 3, along with the coordinate planes, $\{x = 0\}$, $\{y = 0\}$, and $\{z = 0\}$. We label the regions as follows:

$$
\begin{aligned}
S_0 &= \{\dot{x} < 0, \dot{y} < 0, \dot{z} < 0\}, & S_1 &= \{\dot{x} < 0, \dot{y} < 0, \dot{z} > 0\}, \\
S_2 &= \{\dot{x} < 0, \dot{y} > 0, \dot{z} > 0\}, & S_3 &= \{\dot{x} < 0, \dot{y} > 0, \dot{z} < 0\}, \\
S_4 &= \{\dot{x} > 0, \dot{y} < 0, \dot{z} < 0\}, & S_5 &= \{\dot{x} > 0, \dot{y} > 0, \dot{z} < 0\}, \\
S_6 &= S_{6H} \cup S_{6C} = \{\dot{x} > 0, \dot{y} < 0, \dot{z} > 0\}, & S_7 &= \{\dot{x} > 0, \dot{y} > 0, \dot{z} > 0\}.
\end{aligned}
\tag{4.7}
$$

All regions S_i are simply connected, with the exception of S_6 which is the union of two simply-connected components: one which contains the tumor-free equilibrium H, and is denoted by S_{6H}, and one which contains the tumor-present stable equilibrium C, and is denoted by S_{6C}, (see Figure 4).
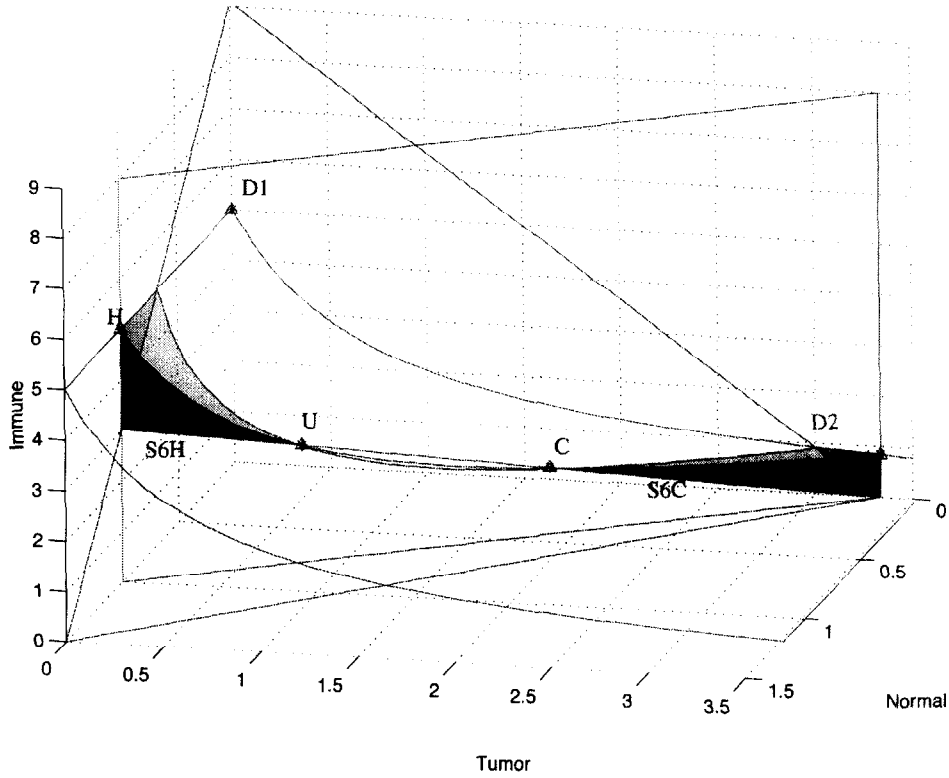
Figure 4. The two outer trapping regions S_6.

The vector field at the interior boundary surfaces

To determine the direction of the vector field on the boundary surfaces, we compute the dot product of the vector field with the outward normal vectors to each of the null-surfaces at a point on the boundary surface. If a surface is the level set of a function, $G(x, y, z) = C$, recall that its outward normal is given by $[\frac{\partial G}{\partial x}, \frac{\partial G}{\partial y}, \frac{\partial G}{\partial z}]$. For clarity, we rewrite the null-surfaces of the nondimensionalized system

$$
\begin{aligned}
N_x &= \{(x, y, z) \mid x + c_4 y = 1\}, \\
N_y &= \{(x, y, z) \mid c_2 x + rby + c_3 z = r\}, \\
N_z &= \left\{(x, y, z) \mid -\frac{1+y}{c_1 y^2 + (c_1 + d - \rho)y + d} + z = 0\right\} = \{-f(y) + z = 0\}.
\end{aligned}
\tag{4.8}
$$

Denoting the vector field given by the system of differential equations in (4.6) by $\mathbf{F} = [\dot{x}, \dot{y}, \dot{z}]$ and the normal to the surface N_i by $N_{i\perp}$, we have

$$
\begin{aligned}
\mathbf{F} \cdot N_{x\perp} &= [\dot{x}, \dot{y}, \dot{z}] \cdot [1, c_4, 0] = c_4 \dot{y}, \\
\mathbf{F} \cdot N_{y\perp} &= [\dot{x}, \dot{y}, \dot{z}] \cdot [c_2, rb, c_3] = c_2 \dot{x} + c_3 \dot{z}, \\
\mathbf{F} \cdot N_{z\perp} &= [\dot{x}, \dot{y}, \dot{z}] \cdot [0, -f'(y), 1] = -f'(y)\dot{y}.
\end{aligned}
\tag{4.9}
$$

In all three equations, we use the fact that the null-surface of a given variable is the set on which its derivative is zero. Furthermore, we note that $f'(y)$ is always strictly negative for the parameter set (4.1). Thus, the sign of $\dot{y}$ and the sign of $c_2 \dot{x} + c_3 \dot{z}$ are sufficient to determine the direction of the vector field at the interior boundary of each region.

The vector field on the coordinate planes

In addition, we note that the coordinate planes $\{x = 0\}$ and $\{y = 0\}$ are invariant under the flow, while the vector field points upward from the plane $\{z = 0\}$ which is not invariant. The
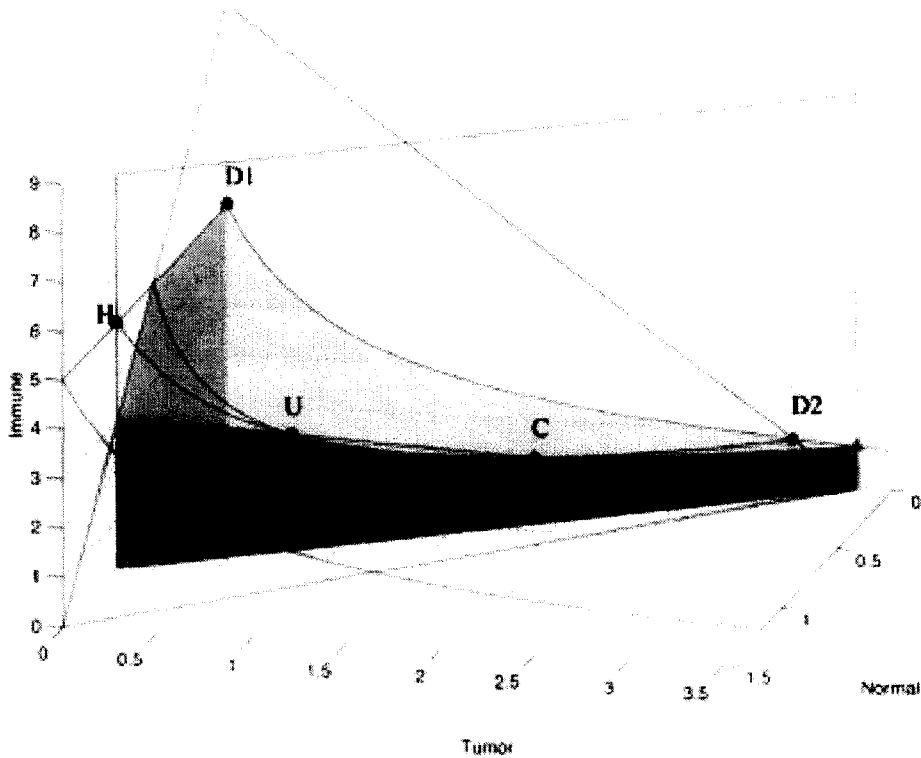
Figure 5. The inner escaping region S_7.
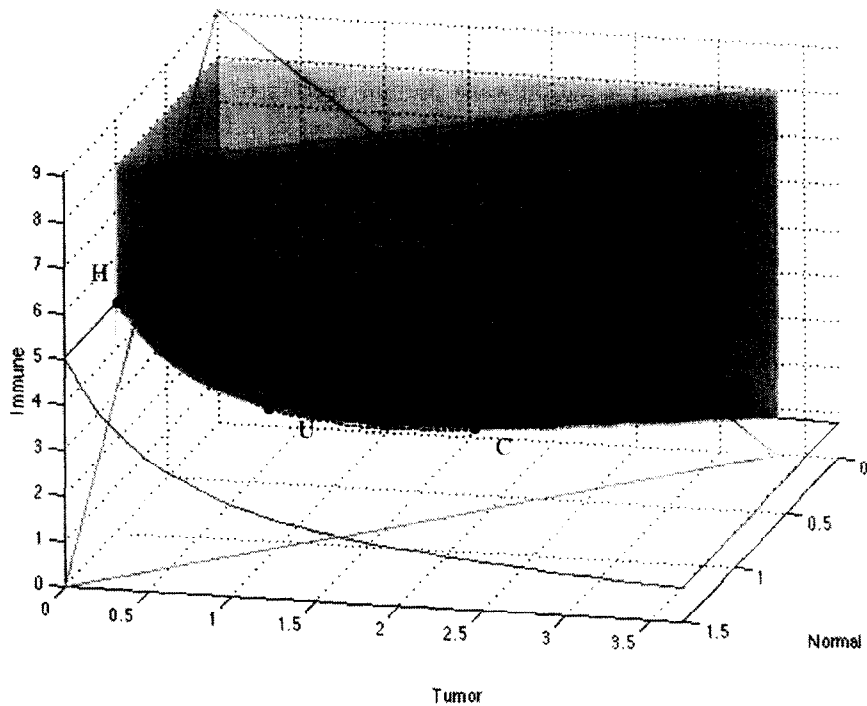
Figure 6. The inner mixed region $T_2 = S_4 \cup S_5$.

z-axis is also invariant under the flow. If $x = 0$ and $y = 0$, the system reduces to a one-dimensional differential equation: $\dot{z} = 1 - dz$, which has a unique stable equilibrium at $D_1 = (0, 0, 1/d)$. On the invariant coordinate planes, the system is two dimensional and, in each case, the reduced system has one stable equilibrium. As stated earlier, all orbits on the yz-plane converge to the

Type 2 "dead" equilibrium D_2 except for those on the z-axis. Similarly, all orbits on the xz-plane converge to the stable healthy equilibrium H. Recall, however, that D_2 is not stable in the full three-dimensional system.

Flow between regions

Since all derivatives are of constant sign in each of the S_i, orbits move toward the respective boundaries of each region. In the unbounded components, S_0, S_1, and S_5, at least two derivatives are negative, and the orbits must move toward one of the null-surfaces. It follows that there can be no unbounded orbits, nor can there be any cycles contained completely within one region. It remains to show that no orbits can move out of one region, but return to it after visiting other regions. We do this by showing that all orbits except those on the z-axis either enter one of the inner regions S_3 or S_6, or converge to one of these regions' vertices. Furthermore, no orbits leave S_3 or S_6. This motivates the classification of the regions into three categories: escaping, mixed, and trapping, described below.

We first consider the two "escaping" regions: the outermost S_0, and the innermost S_7 (see Figure 5). The vector field points out of these regions on each of the boundary components, with the exception of the stable manifolds of D_2 and D_1 in S_7. Therefore, all orbits not on the coordinate planes leave these regions. Next, we consider the mixed regions $T_1 = S_1 \cup S_2$ and $T_2 = S_4 \cup S_5$, the regions in which $\dot{x}$ and $\dot{z}$ are of opposite but constant sign. In particular, we will examine the region T_2 in detail (Figure 6).

In T_2, $\dot{x} > 0$ and $\dot{z} < 0$, so that the region is bounded below by N_z, and has N_x and the xz and yz coordinate planes as its sides. Since $\dot{z} < 0$, all orbits must move downward, and so will eventually reach one of the boundary components. From equations (4.3), we see that the vector field is transverse to all interior boundary surfaces, and points out of T_2 only at $N_z \cap S_5$ and $N_x \cap S_4$, i.e., only at those boundaries shared with one of the three inner regions: S_3, S_{6H}, or S_{6C}. Therefore, all orbits in T_2 must enter one of these three regions. The only exceptions are the orbits initiating on one of the coordinate planes, where the behavior has already been described. This fully describes the nature of the mixed region T_2. The same type of analysis shows that the orbits in T_1 exhibit similar behavior, in that all nonexceptional orbits eventually enter one of the three inner regions.

Finally, the three inner regions are "trapping" regions, since the vector field points inward on all boundary surfaces. All orbits in S_3 converge to the stable interior equilibrium C, except for the single point U at one vertex, which is the unstable interior equilibrium. S_{6H} shares U with S_3 as a boundary vertex. All other points in S_{6H} converge to the healthy stable equilibrium at $H = (1, 1/d, 0)$. S_{6C} shares the unhealthy stable equilibrium C, with S_3, and all points in S_{6C} converge to C except those on its coordinate plane boundary component, $S_{6C} \cap \{x = 0\}$, since these points are in the stable manifold of D_2.

In sum, we have argued the following: with the exception of the z-axis, all orbits in S_0 and S_7 enter T_1 or T_2; all orbits in T_1 or T_2 enter S_3 or S_6, and converge to one of the equilibria. These observations are summarized in Figure 7. We note that the arguments here are geometric and depend on the particular parameter set chosen for the model. On the other hand, since the null-surfaces vary continuously with the parameters, the conclusions drawn here remain valid over a range of parameter sets.

4.4. Basins of Attraction

The discussion above shows that all but a set of measure zero of initial values in the positive octant are on orbits which enter either S_6 or S_3, and converge to either the healthy equilibrium H, or the unhealthy interior stable equilibrium C. We would like to identify the basin of attraction
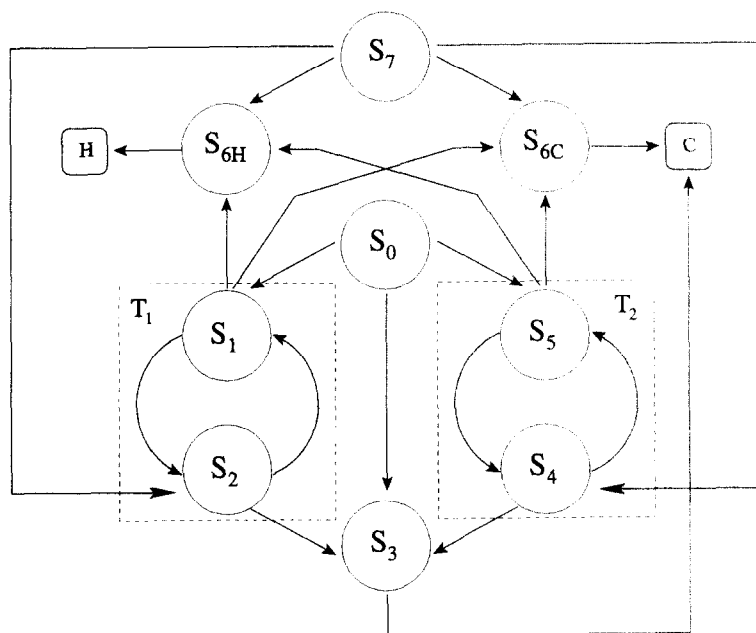
Figure 7. The flow of orbits between regions in phase-space delineated by the null-surfaces. The stable equilibria are H and C, and the exceptional sets are omitted.
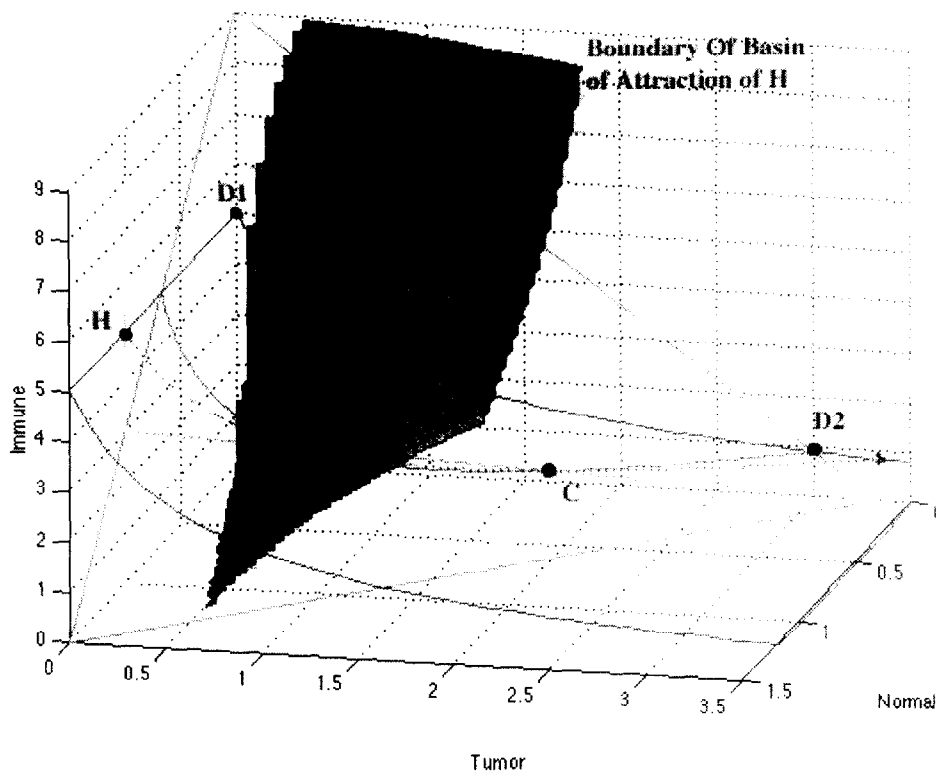

Figure 8. The boundary of the basin of attraction of H for the drug-free system.

of the stable tumor-free equilibrium, as well as the basin of attraction of the "undesirable" stable equilibrium. In particular, we would like to find the boundary between these two regions. The region S_{6H} is completely contained in the basin of attraction, while the regions S_{6C} and S_3 are completely outside the healthy basin. However, the remaining regions intersect both basins. We can numerically approximate where the boundaries of the basins lie, as depicted in Figure 8. Since we have shown that all orbits converge to one of the equilibria, the long-term behavior of an orbit

is completely determined by the basin of attraction in which it originates. Thus, a treatment protocol might be designed which would take advantage of this structure: it is reasonable to define the system to be in a stable, healthy state if it is in the basin of attraction of H. Furthermore, it is reasonable that a mathematical model of such a system should include (at least) two stable attracting states, one of which is considered "healthy" and another which is "diseased". For if this were not the case, we would not observe both types of behavior. A system with only an attracting healthy state would never need to be treated, since it would naturally move back to this state despite any exogenous shock. On the other hand, a system with no attracting healthy state would never stay cured, and no remission from disease would ever be observed. In the following section, we examine how the basin of attraction of H is affected by the addition of a drug to the system.

5. SOLUTIONS WITH DRUG APPROACH SOLUTIONS WITHOUT DRUG

The analysis of the drug-free system (2.3) gives insight into the behavior of the system with a drug applied (2.5). In particular, we are interested in the behavior of the drug-present system after the drug is no longer being actively administered ($v(t) = 0$). In this case, the amount of drug in the system decays exponentially in time. We show in this section that the solutions of the asymptotically autonomous differential equations of the drug-present system (2.5) after the drug has been shut off, have the same behavior as their corresponding limit equations (2.3). That is, the behavior of solutions as the drug in the system decays to zero is continuous, and the limit sets of the drug-free and drug-present systems are the same.

It is sometimes the case that solutions of asymptotically autonomous differential equations can behave quite differently from the solutions of their corresponding limit equations. In [60], we see examples of such systems. Fortunately, our differential equations systems are unlike the examples presented in [60]. In particular, in our case we assume that the time variable t is sufficiently large so that the perturbation of the drug-present case from the drug-free case is very small. Also, we assume that our solution already lies within the basin of attraction of a desirable tumor-free equilibrium point.

In some of the examples presented in [60], the larger the perturbation, the smaller a particular basin of attraction becomes, and the basin eventually disappears when the perturbation is sufficiently large. However, because of the nature of our system, the larger our perturbation (i.e., the greater the amount of drug in the system), the larger the "desirable" basin of attraction of the tumor-free equilibrium point becomes. This basin of attraction may shrink over time as the drug decays, but will never disappear.

We can also write the drug-present system (2.5) in the following nondimensionalized form:

$$
\begin{aligned}
\dot{x} &= x(1 - x) - c_4 xy - f_1(u, t)x, \\
\dot{y} &= ry(1 - by) - c_2 yz - c_3 xy - f_2(u, t)y, \\
\dot{z} &= 1 + \frac{\rho yz}{1 + y} - c_1 yz - dz - f_3(u, t)z,
\end{aligned}
\tag{5.1}
$$

where $f_i(u, t) = a_i(1 - e^{-u(t)})$. If $t = 0$ represents some time after which the administration of the drug has been stopped, then $u(t) = u_0 e^{-d_2 t}$ where $u_0 = u(0)$.

Therefore, the functions f_i are such that for any ε where $0 < \varepsilon \ll 1$, there exists some time T_0 sufficiently large such that for all $t > T_0$, we know $f_i(u, t) < \varepsilon$ for each i. We can view (5.1) as a time-varying perturbation of (4.6), where the perturbation is uniformly less than $\varepsilon > 0$. We therefore analyze the ε-perturbation of (4.6). That is, for time t sufficiently large, the drug-present

system behaves like the following ε-perturbed system of equations:

$$\dot{x} = x(1-x) - c_4xy - \varepsilon x,$$
$$\dot{y} = ry(1-by) - c_2yz - c_3xy - \varepsilon y,$$
$$\dot{z} = 1 + \frac{\rho yz}{1+y} - c_1yz - dz - \varepsilon z. \tag{5.2}$$

Examining the drug-free and the slightly perturbed system, it is clear that the number of equilibrium points for systems (4.6) and (5.2) will be the same, although the relative positions may be shifted by at most ε in some direction. In particular, the ε-perturbed tumor-free equilibrium lies at $(1-\varepsilon, 0, 1/(d+\varepsilon))$. We then look at the Jacobian matrices of the two systems to compare the stability properties of these equilibrium points.

The Jacobian of the drug-free nondimensionalized system (4.6) is given by

$$J_{\text{nodrug}} = \begin{bmatrix} 1 - 2x - c_4y & -c_4x & 0 \\ -c_3y & r - 2bry - c_2z - c_3x & -c_2y \\ 0 & \dfrac{\rho z}{(1+y)^2} - c_1z & \dfrac{\rho y}{1+y} - c_1y - d \end{bmatrix} \tag{5.3}$$

The Jacobian of the ε-perturbed system (5.2) is then given by

$$J_{\text{drug}} = \begin{bmatrix} 1 - 2x - c_4y - \varepsilon & -c_4x & 0 \\ -c_3y & r - 2bry - c_2z - c_3x - \varepsilon & -c_2y \\ 0 & \dfrac{\rho z}{(1+y)^2} - c_1z & \dfrac{\rho y}{1+y} - c_1y - d - \varepsilon \end{bmatrix}. \tag{5.4}$$

That is, we have

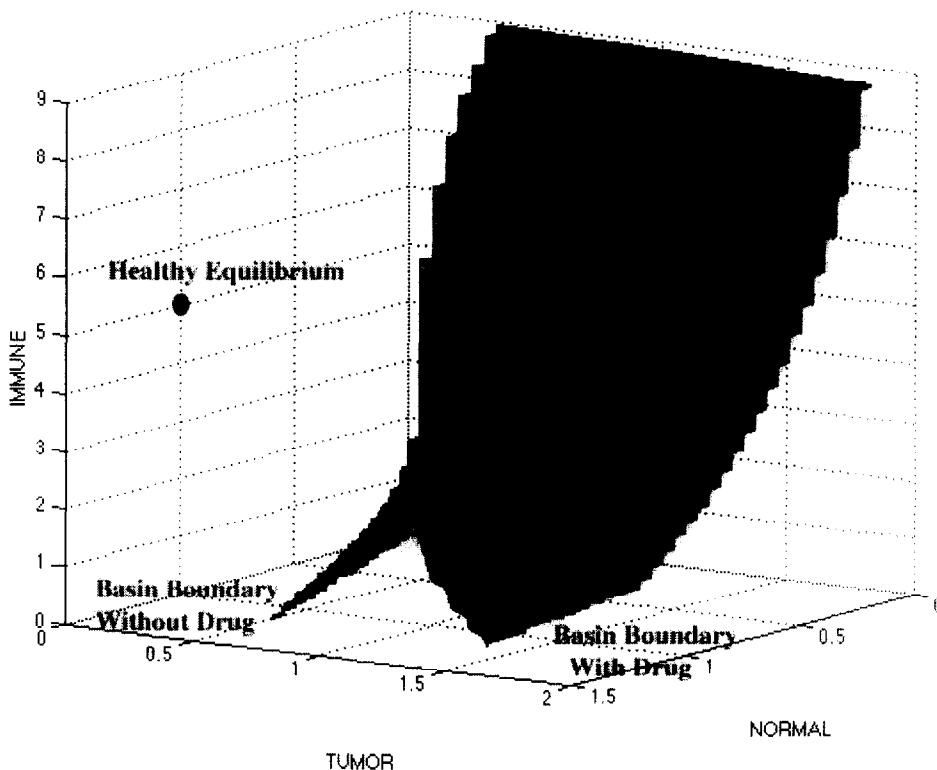$$J_{\text{drug}} = J_{\text{nodrug}} - \varepsilon I, \tag{5.5}$$

Figure 9. A comparison of the healthy basin of attraction for the system with and without drug. The tumor-free equilibrium H is shown.

where I represents the 3×3 identity matrix. Therefore, if the eigenvalues of J_{nodrug} are represented by λ_i, then the eigenvalues of J_{drug} are of the form $\lambda_i - \varepsilon$. Hence, the signs of $\text{Re}(\lambda_i)$ and $\text{Re}(\lambda_i - \varepsilon)$ will be the same for sufficiently small ε, as long as $\text{Re}(\lambda_i) \neq 0$, for all i. Since, we know this is the case for the parameters under consideration, the perturbed system (5.2) and the drug-free system (4.6) have the same stability properties. As $\varepsilon \to 0$, the limit set of (5.2) approaches the limit set of (4.6). Therefore, it is clear that the limit set of (5.1), with u_0 sufficiently small, equals the limit set of (4.6).

To illustrate these ideas, we show in Figure 9 a numerical estimate of the boundaries of the basins of attraction of H, the stable tumor-free equilibrium, for the system both with and without drugs. In the system with drug, the administration of the drug has been stopped at the beginning of the simulation, but some amount of drug is assumed to still be present at the tumor site. Note that the boundary of the basin of attraction for H is further away from H when the drug is in the system, i.e., the addition of the drug *enlarges* the basin of attraction of H. The difference in the two basins is most noticeable when the immune population is small, with the basin boundaries approaching each other as the immune population z increases.

6. OPTIMAL THERAPY PROTOCOLS

In this section, we add the effect of chemotherapy treatments to our system, and we use optimal control theory to look for an improved administration protocol. Our control problem consists of determining the function $v(t)$ (representing the chemotherapy administration schedule) that will kill off the tumor cell population as effectively as possible, with the constraint that we do not also kill too many normal cells.

The general optimal control problem can be stated as follows. Find the control variable $v(t)$, and the possibly free final time t_f, that minimize the objective function

$$J(v, t_f) = \Phi(\mathbf{x}(t_f), t_f), \tag{6.1}$$

subject to the state equations

$$\dot{\mathbf{x}}(t) = f(\mathbf{x}(t), v(t), t), \qquad t_0 \leq t \leq t_f, \tag{6.2}$$

and a state constraint

$$g(\mathbf{x}(t)) \geq 0. \tag{6.3}$$

In our experiments, we choose to specify the final time t_f in order to reflect a standard four to five month treatment process. In the future, we may choose to examine the outcome if we leave t_f free. In our previous work [1], we chose a fairly simple objective function, which represented minimizing the number of tumor cells at some specified final time t_f. The units of cells were normalized so that the carrying capacity of normal cells was 1 (i.e., $b_2 = 1$); we then required that the number of normal cells stay above three-fourths of the carrying capacity, or $x(t) \geq 0.75$ for all t. In the language of optimal control theory, our objective function and our constraint were given by

- original objective function (minimize tumor burden at final time)

$$J(t_f) = y(t_f), \tag{6.4}$$

- constraint (keep normal cells above threshold)

$$x(t) \geq 0.75, \qquad 0 \leq t \leq t_f, \tag{6.5}$$

subject to the state equations given in (2.5).

With this simple objective function, the tumor cell population was indeed lower at t_f with optimal control chemotherapy than it was with traditional pulsed chemotherapy. However, fairly large oscillations in the tumor cell population were also induced. This motivated us to find alternate objective functions that would allow us to minimize the tumor cell population while keeping the oscillations under control.

The new set of objective functions we currently employ for the experiments we present in this paper are a weighted combination of the tumor burden at the final time, along with the total tumor burden summed over the course of treatment, and the maximum tumor burden achieved during the course of treatment. The new objective function therefore has the form

$$J(t_f) = w_1 y(t_f) + w_2 \int_0^{t_f} y(t)\, dt + w_3 \max_{t \in (t_0, t_f)} y(t), \qquad (6.6)$$

where w_i are weighting constants. For the set of experiments we present, we set $w_1 = 1500$. $w_2 = 150$, $w_3 = 1000$. We keep the same constraint as in (6) on the level of the normal cell population.

When employing this new objective function, oscillations in the solution are indeed decreased as compared to the original simpler objective function that only minimized total tumor burden at the final time.
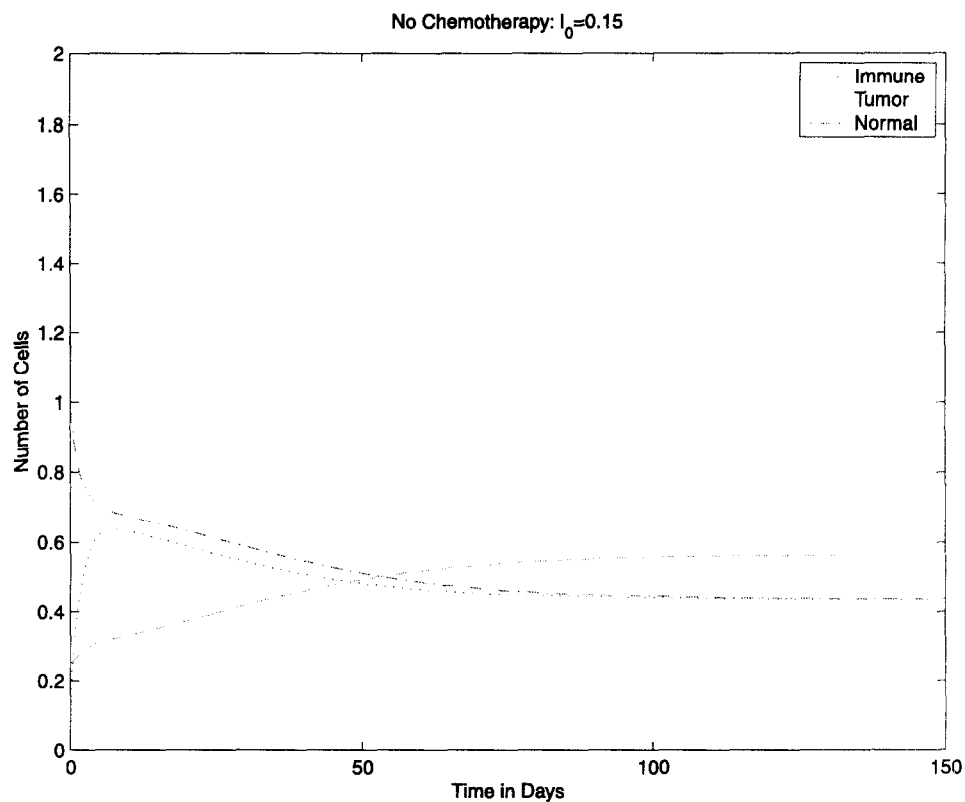
7. NUMERICAL SOLUTIONS

For the numerical experiments we present, we used a direct collocation method to solve the optimal control problem formulated in Section 6, implemented with the software DIRCOL v1.2 [61]. The algorithm is sensitive to user input at various stages; in particular, it fails if the initial estimates of the state variables and the control variable are not close enough to optimal values. The grid of points at which the control is given is also crucial to the success of the algorithm.

Optimal control theory shows that for our system of equations, we should expect the solutions to the optimal control problem to be "bang-bang". That is, a candidate protocol for an optimal administration of the drug would deliver either full dose or no dose, and all that needs to be determined is when to turn the dosage on and off. See [1] for details of this analysis. The numerical solutions we achieve are indeed bang-bang. Although there is no guarantee that with this approach the solutions are globally optimal, they do show themselves to be superior to traditional pulsed chemotherapy.

The parameter set we are working with is in a region where we have two stable equilibria: one with a large tumor burden, and one with zero tumor burden. Our goal is to drive the system toward the zero tumor burden equilibrium point. We test two separate cases, both of which place us initially in the basin of attraction of the large tumor burden equilibrium point. That is, without the intervention of a drug, the patient will not survive. We start with two different initial immune system strengths. One set of experiments starts with $I(0) = z(0) = 0.10$, and the other set starts with slightly stronger immune system populations at $I(0) = z(0) = 0.15$.

From Figure 10, we see that when the system progresses naturally without any drug intervention, the tumor burden overwhelms the system, while the normal cell population quickly decreases to below survival levels.

Standard protocol is to administer the drug for a short time, on the order of several hours, with periodically repeated treatments every few weeks. In Figure 11, we see the effects of traditional pulsed chemotherapy. In the case of the slightly stronger immune system, the chemotherapy treatment is sufficient to push the system into the basin of attraction of the desirable tumor-free equilibrium point. This means that even after the medicines are turned off, the tumor burden will continue to decrease toward zero. However, with a slightly weakened immune system, it is clear that although traditional treatment can keep the tumor burden bounded while treatment

No Chemotherapy: $I_0 = 0.15$

(a) $I(0) = z(0) = 0.15$.

No Chemotherapy: $I_0 = 0.1$
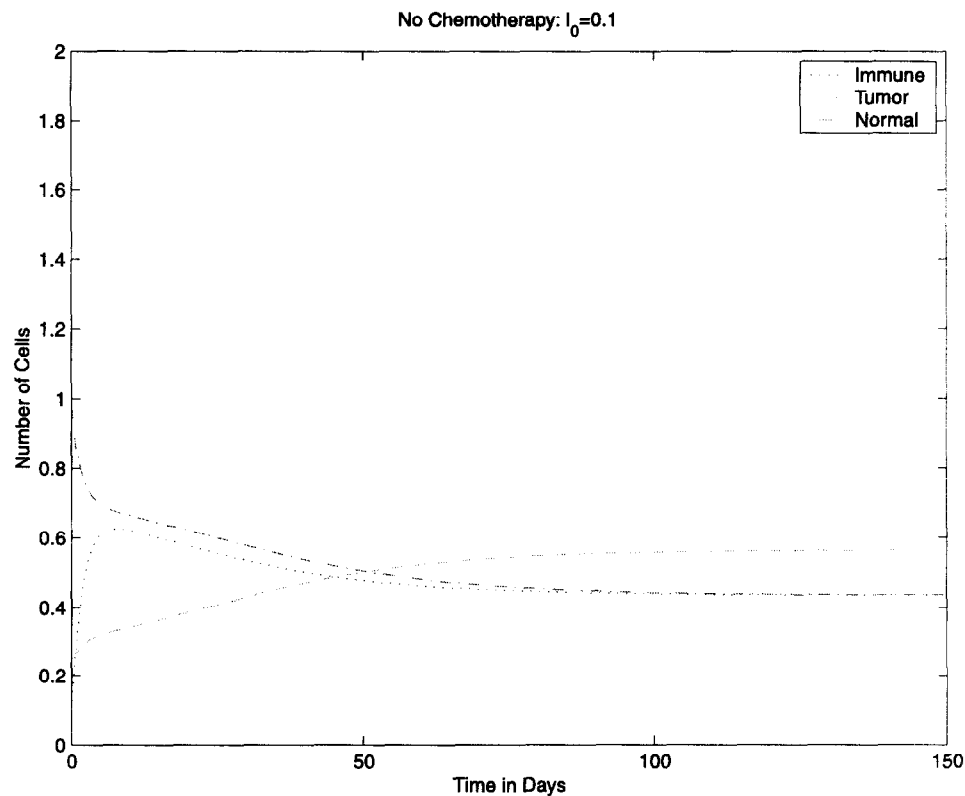
(b) $I(0) = z(0) = 0.10$.

Figure 10. Cancer progression, no medication.

Traditional pulsed chemotherapy: $I_0 = 0.15$

(a) $I(0) = x(0) = 0.15$.

Traditional pulsed chemotherapy: $I_0 = 0.1$
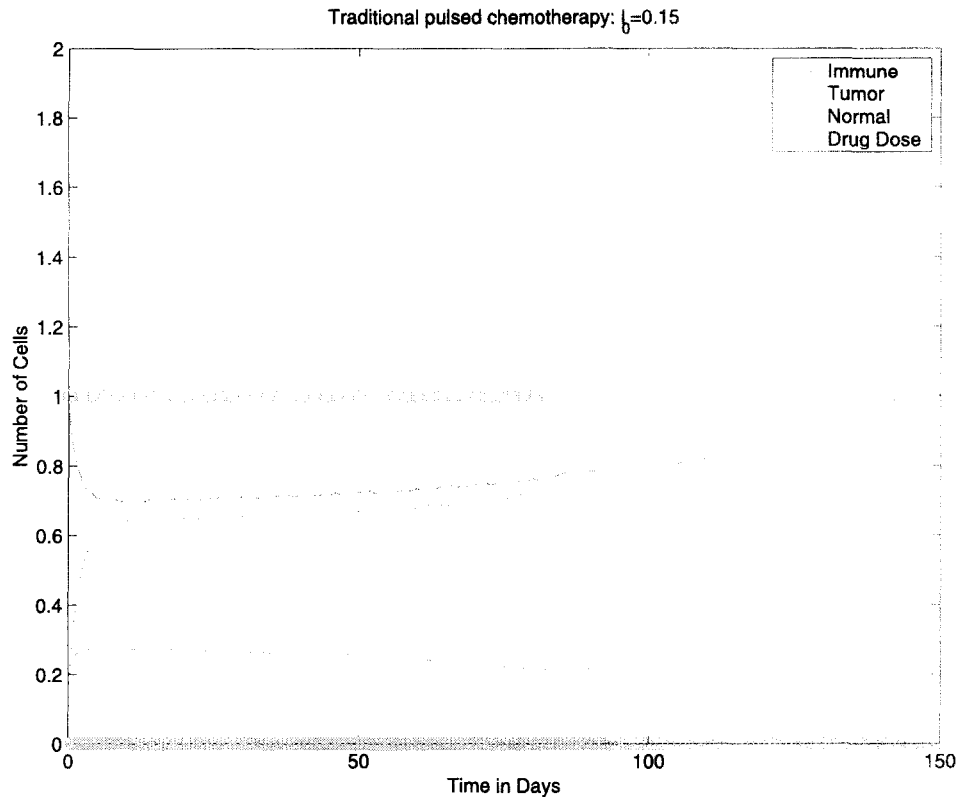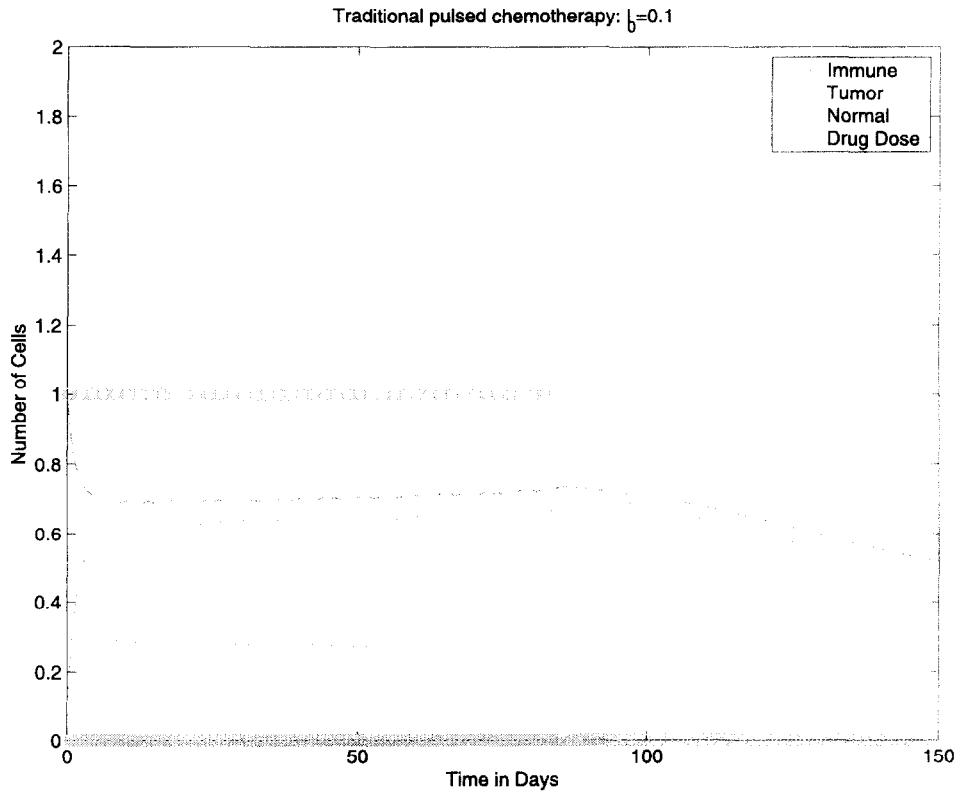

(b) $I(0) = x(0) = 0.10$.

Figure 11. Cancer progression, pulsed chemotherapy.

Optimal control chemotherapy: I_0=0.15

(a) $I(0) = z(0) = 0.15$.

Optimal control chemotherapy: I_0=0.1
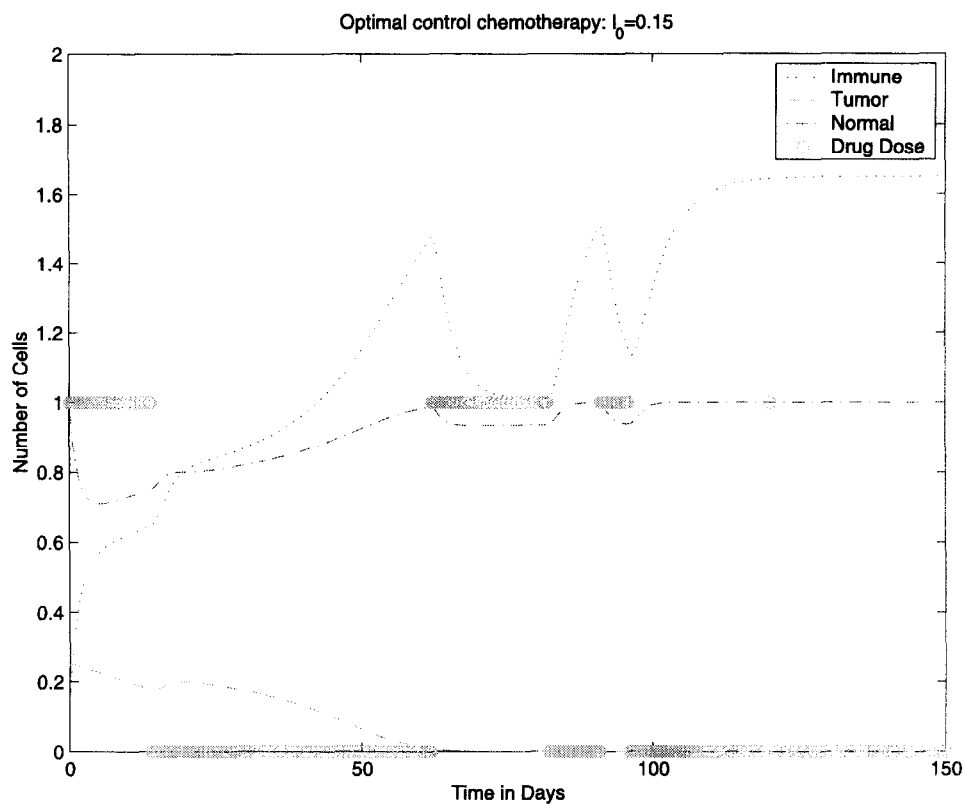
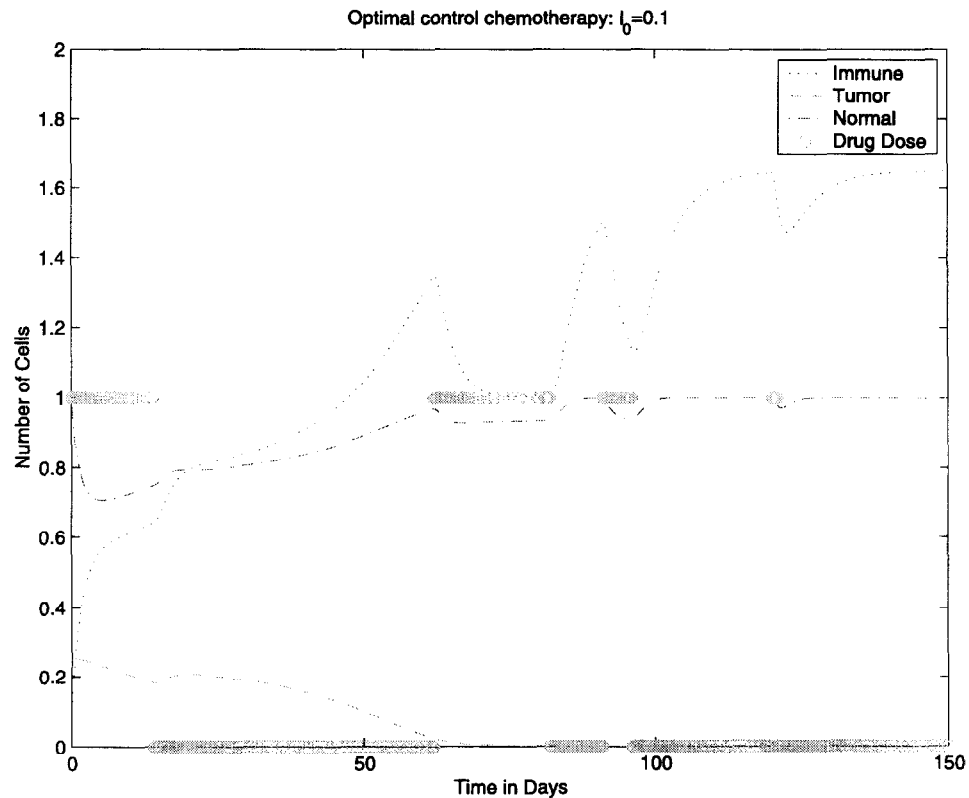(b) $I(0) = z(0) = 0.10$.

Figure 12. Cancer progression, optimal control chemotherapy.

is being administered, once the medicines are stopped the tumor begins to increase in size again, and heads toward the undesirable large tumor equilibrium point.

This is where optimal control proves to be of some use. The protocol suggested by the optimal control algorithm dictates that the drug be administered continuously over relatively long periods of time—on the order of days. Figure 12 shows the evolution of the system with the optimal control treatment administered. In both the weak and strong initial immune strength cases, optimal control therapy is superior to traditional pulsed therapy in the sense that the tumor burden is driven to low levels more quickly, and the normal cell population stays at higher levels for longer periods of time. Additionally, however, for the weaker immune system case, traditional therapy fails to bring the system into the desirable basin of attraction at all (see Figure 11), whereas the optimal control protocol does successfully push the system into the zero-tumor-burden basin of attraction. Therefore, in both the weak and strong immune system cases, the medicines eventually can be shut off, and the tumor will continue to decrease to zero without further intervention.

As stated earlier, these solutions are not guaranteed to be globally optimal and it may be possible to find treatment protocols that are just as effective but use even less total drug. However, even these locally optimal solutions show themselves to be superior to traditional pulsed protocols.

We note here that the total amount of medicine administered for the optimal control protocol is no more than the total amount of medicine administered for the pulsed protocol. Also, in both cases, the maximum dose administered is the same. Therefore, the only difference between the two protocols is in the timing of the administration of the drug.

8. CONCLUSIONS

In the particular parameter range we examined, the limit sets of all points consist of only one equilibrium. Therefore, chemotherapeutic treatment can be stopped as soon as an orbit enters the basin of attraction of the tumor-free equilibrium. The structure of the limit sets depends on the configuration of the null-surfaces of the system. This configuration changes continuously as the parameters are varied, so that the relevant properties of the limit sets will remain the same for an open set of parameter values. In other words, the nonexistence of limit cycles and the boundedness of orbits are robust features under small parameter perturbations.

In a future work, we plan to investigate the efficacy of exploiting this phase-space structure in the development of improved optimal control objective functions. Our current objective function requires that total tumor burden is minimized while the normal cell population is constrained to stay above certain healthy levels. We plan to explore modifying the objective so that, instead, the time it takes to move into the basin of attraction of a healthy equilibrium is minimized. This could be a nontrivial task, since it involves estimating the boundary of the basin of attraction in a computationally effective way.

The model itself is meant as an example, and is quite simple. In the future, we plan to perform a similar analysis on models which include drug resistance and more specific immune cell types. Some interesting models have been developed which incorporate the spatial heterogeneity of tumors. We would like to apply phase-space analysis and optimal control to these types of models as well, in order to take into account such important physiological processes as drug diffusion, nutrient consumption, and the development of vasculature in solid tumors.

REFERENCES

1. L. de Pillis and A. Radunskaya, A mathematical tumor model with immune resistance and drug therapy: An optimal control approach, *Journal of Theoretical Medicine* **3**, 79–100 (2001).
2. V. Kuznetsov, I. Makalkin, M. Taylor and A. Perelson, Nonlinear dynamics of immunogenic tumors: Parameter estimation and global bifurcation analysis, *Bull. of Math. Bio.* **56** (2), 295–321 (1994).
3. V. Kuznetsov and G. Knott, Modelling tumor regrowth and immunotherapy, *Mathl. Comput. Modelling* **33** (12/13), 1275–1287 (2001).

4. N. Bellomo and L. Preziosi, Modelling and mathematical problems related to tumor evolution and its interaction with the immune system, *Mathl. Comput. Modelling* **32** (3/4), 413–452 (2000).

5. B. Firmani, L. Guerri and L. Preziosi, Tumor/immune system competition with medically induced activation/deactivation, *Mathematical Models and Methods in Applied Sciences* **4** (9), 491–512 (1999).

6. M. Owen and J. Sherratt, Mathematical modelling macrophage dynamics in tumors, *Mathematical Models and Methods in Applied Sciences* **9** (4), 513–539 (1999).

7. D. Kirschner and J. Panetta, Modelling immunotherapy of the tumor-immune interaction, *Journal of Mathematical Biology* **37** (3), 235–252 (1998).

8. S. Michelson and J. Leith, Host response in tumor growth and progression, *Invasion and Metastasis* **16** (4-5), 235–246 (1996).

9. F. Nani and M. Oguztoreli, Modelling and simulation of Rosenberg-type adoptive cellular immunotherapy, *IMA Journal of Mathematics Applied in Medicine and Biology* **11** (2), 107–147 (1994).

10. J.A. Adam, The dynamics of growth-factor-modified immune response to cancer growth: One-dimensional models, *Mathl. Comput. Modelling* **17** (3), 83–106 (1993).

11. V. Kuznetsov and I. Makalkin, Bifurcation-analysis of mathematical-model of interactions between cytotoxic lymphocytes and tumor-cells—Effect of immunological amplification of tumor-growth and its connection with other phenomena of oncoimmunology, *Biofizika* **37** (6), 1063–1070 (1992).

12. S. Clare, F. Nakhlis and J. Panetta, Molecular biology of breast cancer metastasis. The use of mathematical models to determine relapse and to predict response to chemotherapy in breast cancer, *Breast Cancer Research* **2** (6), 430–435 (2000).

13. E. Shochat, D. Hart and Z. Agur, Using computer simulations for evaluating the efficacy of breast cancer chemotherapy protocols, *Mathematical Models and Methods in Applied Sciences* **9** (4), 599–615 (1999).

14. F. Nani and M. Oguztoreli, Modelling and simulation of chemotherapy of haematological and gynaecological cancers, *IMA Journal of Mathematics Applied in Medicine and Biology* **16** (1), 39–91 (1999).

15. M. Costa and J. Boldrini, Chemotherapeutic treatments: A study of the interplay among resistance, toxicity and recuperation from side effects, *Bulletin of Mathematical Biology* **59** (2), 205–232 (1997).

16. J. Panetta, A logistic model of periodic chemotherapy with drug resistance, *Appl. Math. Lett.* **10** (1), 123–127 (1997).

17. J. Panetta, A mathematical model of periodically pulsed chemotherapy: Tumor recurrence and metastasis in a competitive environment, *Bulletin of Mathematical Biology* **58** (3), 425–447 (1996).

18. M. Costa, J. Boldrini and R. Bassanezi, Chemotherapeutic treatments involving drug-resistance and level of normal-cells as a criterion of toxicity, *Mathematical Biosciences* **125** (2), 211–228 (1995).

19. J.A. Adam and J. Panetta, A simple mathematical model and alternative paradigm for certain chemotherapeutic regimens, *Mathl. Comput. Modelling* **22** (8), 49–60 (1995).

20. H. Knolle, *Cell Kinetic Modelling and the Chemotherapy of Cancer*, Springer-Verlag, Berlin. (1988).

21. B.F. Dibrov, A.M. Zhabotinsky, Y.A. Neyfakh, M.P. Orlova and L.I. Churikova, Mathematical model of cancer chemotherapy. Periodic schedules of phase-specific cytotoxic-agent administration increasing the selectivity of therapy, *Mathematical Biosciences. An International Journal* **73** (1), 1–31 (1985).

22. A. Petrovski, J. McCall and E. Forrest, An application of genetic algorithms to optimization of cancer chemotherapy, *International Journal of Mathematics in Education, Science and Technology* **29** (3), 377–388 (1998).

23. J. Boldrini and M. Costa, The influence of fixed and free final time of treatment on optimal chemotherapeutic protocols, *Mathl. Comput. Modelling* **27** (6), 59–72 (1998).

24. M. Costa and J. Boldrini, Conflicting objectives in chemotherapy with drug resistance, *Bulletin of Mathematical Biology* **59** (4), 707–724 (1997).

25. A. Swierniak, A. Polanski and M. Kimmel, Optimal control problems arising in cell-cycle-specific cancer chemotherapy, *Journal of Cell Proliferation* **29**, 117–139 (1996).

26. A. Swierniak and A. Polanski, Irregularity in scheduling of cancer chemotherapy, *Applied Mathematics and Computer Science* **4** (2), 263–271 (1994).

27. A. Swierniak, Some control problems for simplest differential models of proliferation cycle, *Applied Mathematics and Computer Science* **4** (2), 223–232 (1994).

28. J. Murray, Optimal drug regimens in cancer-chemotherapy for single drugs that block progression through the cell-cycle, *Mathematical Biosciences* **123** (2), 183–213 (1994).

29. A. Swierniak and Z. Duda, Singularity of optimal-control in some problems related to optimal chemotherapy, *Mathl. Comput. Modelling* **19** (6–8), 255–262 (1994).

30. M. Costa, J. Boldrini and R. Bassanezi, Optimal chemotherapy. A case-study with drug-resistance, saturation effect, and toxicity, *IMA Journal of Mathematics Applied in Medicine and Biology* **11** (1), 45–59 (1994).

31. R.B. Martin, Optimal control drug scheduling of cancer chemotherapy, *Automatica. The Journal of IFAC, the International Federation of Automatic Control* **28** (6), 1113–1123 (1992).

32. J.M. Murray, Optimal control for a cancer chemotherapy problem with general growth and loss functions, *Mathematical Biosciences. An International Journal* **98** (2), 273–287 (1990).

33. R.B. Martin, M.E. Fisher, R.F. Minchin and K.L. Teo, A mathematical model of cancer chemotherapy with an optimal selection of parameters, *Mathematical Biosciences. An International Journal* **99** (2), 205–230 (1990).

34. G.W. Swan, Optimal control analysis of a cancer chemotherapy problem, *IMA (Institute of Mathematics and its Applications) Journal of Mathematics Applied in Medicine and Biology* **4** (2), 171–184 (1987).

35. G.W. Swan, Optimal control applications in the chemotherapy of multiple myeloma, *IMA Journal of Mathematics Applied in Medicine and Biology* **2** (3), 139–160 (1985).

36. M. Eisen, *Mathematical Models in Cell Biology and Cancer Chemotherapy*, Springer-Verlag, Berlin, (1979).

37. A. Swierniak and J. Smieja, Cancer chemotherapy optimization under evolving drug resistance, *Nonlinear Analysis—Theory, Methods and Applications* **47** (1), 375–386 (2001).

38. D. Barbolosi and A. Iliadis, Optimizing drug regimens in cancer chemotherapy: A simulation study using a pk-pd model, *Computers in Biology and Medicine* **31** (3), 157–172 (2001).

39. A. Matveev and A. Savkin, Optimal chemotherapy regimens: Influence of tumours on normal cells and several toxicity constraints, *IMA Journal of Mathematics Applied in Medicine and Biology* **18** (1), 25–40 (2001).

40. A. Iliadis and D. Barbolosi, Optimizing drug regimens in cancer chemotherapy by an efficacy-toxicity mathematical model, *Computers and Biomedical Research* **33** (3), 211–226 (2000).

41. K. Fister and J. Panetta, Optimal control applied to cell-cycle-specific cancer chemotherapy, *SIAM Journal on Applied Mathematics* **60** (3), 1059–1072 (2000).

42. J. Boldrini and M. Costa, Therapy burden, drug resistance, and optimal treatment regimen for cancer chemotherapy, *IMA Journal of Mathematics Applied in Medicine and Biology* **17** (1), 33–51 (2000).

43. M. Owen and J. Sherratt, Modelling the macrophage invasion of tumours: Effects on growth and composition, *IMA Journal of Mathematics Applied in Medicine and Biology* **15**, 165–185 (1998).

44. F. Nani and H. Freedman, A mathematical model of cancer treatment by immunotherapy, *Mathematical Biosciences* **163**, 159–199 (2000).

45. P. van den Driessche and M. Zeeman, Three-dimensional competitive Lotka-Volterra systems with no periodic orbits, *SIAM Journal on Applied Mathematics* **58** (1), 227–234 (1998).

46. F. DeOca and M. Zeeman, Extinction in nonautonomous competitive Lotka-Volterra systems, *Proceedings of the American Mathematical Society* **124** (12), 3677–3687 (1996).

47. F. DeOca and M. Zeeman, Balancing survival and extinction in nonautonomous Lotka-Volterra systems, *Journal of Mathematical Analysis and Applications* **192** (2), 360–370 (1995).

48. M. Zeeman, Extinction in competitive Lotka-Volterra systems, *Proceedings of the American Mathematical Society* **123** (1), 87–96 (1995).

49. E. Zeeman and M. Zeeman, On the convexity of carrying simplices in competitive Lotka-Volterra systems, In *Differential Equations, Dynamical Systems and Control Science*, (Edited by K. Elworthy, W. Everitt and E. Lee), pp. 353–364, Marcel Dekker, New York, (1993).

50. M. Hirsch, Systems of differential equations that are competitive or cooperative. iii: Competing species. *Nonlinearity* **1**, 51–71 (1988).

51. R. Prehn, Stimulatory effects of immune-reactions upon the growths of untransplanted tumors, *Cancer Research* **54** (4), 908–914 (1994).

52. V. Vaidya and F. Alexandro, Jr., Evaluation of some mathematical models for tumor growth, *International Journal of Bio-Medical Computing* **13**, 19–35 (1982).

53. D. Hart, E. Shochat and Z. Agur, The growth law of primary breast cancer as inferred from mammography screening trials data, *British Journal of Cancer* **78** (3), 382–387 (1998).

54. R. Borrelli and C. Coleman, *Differential Equations: A Modelling Perspective*, John Wiley and Sons, (1998).

55. J. Rieker, Conversations, Physician with Pomona Valley Hospital, Pomona, CA (1999).

56. S. Kusama, J. Spratt, W. Donegan, F. Watson and C. Cunningham, The gross rates of growth of human mammary carcinoma, *Cancer* **30** (2), 594–599 (1972).

57. C. Arnerøv, S. Emdin, B. Lundgren, G. Roos, I. Søderstrøm, L. Bjersing, C. Norberg and K. Ångquist, Breast carcinoma growth rate described by mammographic doubling time and S-phase fraction: Correlations to clinical and histopathologic factors in a screened population, *Cancer* **70** (7), 1928–1934 (1992).

58. G. Steel, *Growth Kinetics of Tumors*, Oxford University Press, Oxford, (1977).

59. L. Perko, *Differential Equations and Dynamical Systems*, Springer-Verlag, New York, (1993).

60. H. Thieme, Asymptotically autonomous differential equations in the plane, *Rocky Mountain Journal of Mathematics* **24** (1), 351–379 (1994).

61. O. von Stryk, User's guide for DIRCOL: A direct collocation method for the numerical solution of optimal control problems, Lehrstuhl M2 Numerische Mathematik, Technische Universität, München, copyright (C) 1994–1999 (1999).